FINAL REPORT

Structural Enhancements to Adapt to Impacts of Climate Change

Date: June 2016

Osman E. Ozbulut, Ph.D., Assistant Professor, University of Virginia
Sherif Daghash, Graduate Student, University of Virginia
Muhammad M. Sherif, Graduate Student, University of Virginia
Devin K. Harris, Ph.D., Assistant Professor, University of Virginia

Prepared by:

Department of Civil and Environmental Engineering
University of Virginia
351 McCormick Rd Thornton Hall
Charlottesville, VA 22904

Prepared for:
Virginia Center for Transportation Innovation and Research
530 Edgemont Road
Charlottesville, VA 22903

1. Report No.	2. Government Accession No.	3. Recipient's Catalog No.
4. Title and Subtitle Structural Enhancements to Adapt to Impacts of Climate Change		**5. Report Date**
		6. Performing Organization Code
7. Author(s) Osman E. Ozbulut, Ph.D, Sherif Daghash, Muhammad M. Sherif, Devin K. Harris, Ph.D		**8. Performing Organization Report No.**
9. Performing Organization Name and Address Department of Civil and Environmental Engineering University of Virginia 351 McCormick Rd Thornton Hall Charlottesville, VA 22904		**10. Work Unit No. (TRAIS** **11. Contract or Grant No.** DTRT13-G-UTC33
12. Sponsoring Agency Name and Address US Department of Transportation Office of the Secretary-Research UTC Program, RDT-30 1200 New Jersey Ave., SE Washington, DC 20590		**13. Type of Report and Period Covered** Final 10/01/14 – 05/31/16 **14. Sponsoring Agency Code**

15. Supplementary Notes

16. Abstract

With the apparent evolution towards more extreme weather including hurricanes and tropical storms, state transportation agencies are realizing the need for adaptive infrastructure systems that can react and adapt to these events. However, dramatic changes in practices such as reconstruction or shifting population centers is extremely difficult to achieve. More rational alternatives include solutions that adapt existing infrastructure to tolerate these events. From the perspective of structural systems, this includes updating design with new durable and robust materials and rehabilitating existing structures with retrofits that extend service life. In addition to enhancing the longevity and performance of structural systems, these solutions need to be cost effective. The objective of this research is to reduce the vulnerability of civil infrastructure systems in light of expected climate change and associated increase in extreme weather events by developing and integrating advanced composite materials into sustainable structural design.

Shape memory alloys (SMAs) are a class of metallic alloys that can recover large strains upon load removal with minimal residual deformations. Besides their ability to recover large deformations, SMAs possess excellent corrosion resistance, good energy dissipation capacity, and high fatigue properties. SMA materials have superelastic properties that can overcome the brittle behavior of carbon or glass FRP and provide ductility. SMAs can also enhance the damping capacity and toughness of the matrix and provide re-centering ability. This study explores the use of superelastic SMA fibers in developing advanced composites that can be integrated into structural design to enhance the performance of civil infrastructure systems subjected to extreme weather events. First, SMA materials are used to reinforce a thermoset polymer matrix to produce SMA Fiber Reinforced Polymers. Then, the use of SMA fiber in cementitious composites are explored. Experimental tests are conducted to assess the performance of the developed composites and the test results are analyzed in detail. Results from this investigation show that SMA fibers can provide some advantages over traditional fibers such as ability to experience larger deformations, crack control, and minimizing permanent damages and residual displacements.

17. Key Words	18. Distribution Statement
Advanced composites, fiber reinforced polymer (FRP), shape memory alloys (SMAs), superelasticity, cyclic behavior, mortar	No restrictions. This document is available from the National Technical Information Service, Springfield, VA 22161

19. Security Classif. (of this report)	20. Security Classif. (of this page)	21. No. of Pages	22. Price
Unclassified	Unclassified	XX	

DISCLAIMER

The contents of this report reflect the views of the authors, who are responsible for the facts and the accuracy of the information presented herein. This document is disseminated under the sponsorship of the U.S. Department of Transportation's University Transportation Centers Program, in the interest of information exchange. The U.S. Government assumes no liability for the contents or use thereof.

TABLE OF CONTENTS

LIST OF FIGURES

LIST OF TABLES

INTRODUCTION

Climate change is expected to considerably impact the health of civil infrastructure systems. As extreme weather events, hurricanes, tropical storms, prolonged intense temperatures occur more frequently, state transportation agencies are in need of strategies to avoid, minimize or mitigate potential consequences. The potential adverse effects of extreme weather events on civil infrastructure include but not limited to premature deterioration of infrastructure system; extra stresses through thermal expansion in bridges; damage to roads, coastal highways, and tunnels due to heavy precipitation and increased runoff; increased fatigue problems in sign, signal and bridge structures due to extreme winds; and increased scouring problems in bridges due to higher stream runoff and rising sea levels [1].

This research aims to reduce the vulnerability of civil infrastructure systems in light of expected climate change and associated increase in extreme weather events by developing advanced composites that can be integrated into structural design. The new composites studied here are based on shape memory alloys (SMAs). SMAs have unique properties such as high strength, very good fatigue and corrosion resistance, large damping capacity, re-centering capability, and ability to undergo large deformations. Due to the change in their magnetism with strain during superelastic deformation, SMAs can also offer the capability of self-sensing in structural health monitoring. This study investigates the development of two types of advanced composites: (i) SMA Fiber Reinforced Polymers and (ii) SMA Fiber Reinforced Mortar. The use of smart composites in infrastructure systems is expected to enhance system resilience to extreme events and provide a supplement benefit of damage detection for civil infrastructure.

SHAPE MEMORY ALLOY FIBER REINFORCED POLYMERS

PROBLEM

In recent years, fiber reinforced polymers (FRPs) have gained increased acceptance in numerous civil engineering applications [2]. FRPs are considered as attractive materials for construction and strengthening applications due to their high strength-to-weight ratio, high corrosion resistance, and good durability. On the other hand, conventional FRPs do not exhibit ductile behavior, resulting in a limited ability to dissipate strain energy with ultimate tensile strain between 2-3 % [2]. The catastrophic brittle failure of FRPs with low toughness capacity is considered one of the main drawbacks of this material. FRPs also have a limited fatigue strength compared to traditional metallic materials. As a result, most design codes limited the FRP service stress levels to 35%, on average, of its ultimate strength [3]. The limitation on service stress significantly offsets many of the economic advantages of the FRPs.

Different types of fibers have been used to fabricate a wide variety of FRP composites with different behaviors and applications. Carbon (C) and glass (G) fibers have received the most attention in the FRP industry with numerous researchers studying the mechanical behavior of carbon fiber reinforced polymer (CFRP) and glass fiber reinforced polymer (GFRP) composites.

Shape memory alloys (SMAs) are a relatively new class of metallic alloys that can memorize their original shape and recover large strains. The shape recovery in SMAs occurs either mechanically upon load removal (superelastic SMAs), or thermally by heating the material after removal of loads (shape memory effect SMAs). Superelastic SMAs can recover strains between 6-8 % with minimal residual deformations. Since the loading and unloading trajectories do not coincide, a hysteresis loop occurs, exhibiting inherent energy dissipation capabilities [9]. They also possess excellent corrosion resistance and good fatigue properties. Due to all of the previously mentioned advantages, SMAs have been utilized in many applications in different fields including biomedical, aerospace, automotive, and construction. SMAs were first used in medical applications such as heart surgeries, artificial muscles, and dentistry [10,11]. In the aerospace and industrial fields, SMAs applications have included adaptive wings with adjustable shapes, temperature control systems, and telephone antennas [12].

In structural applications, SMAs are used in the form of wires, cables or rods. For example, SMA wires were evaluated as damping systems for tall structures, in seismic isolation systems and in retrofitting historical structures [13-16]. SMA rods were used in self-centering buckling restrained bracing systems for energy dissipation and recentering purposes and in near-surface-mounted applications as an alternative to FRPs for strengthening concrete structures [17,18]. More recently, SMA cables were experimentally investigated and found to provide the high strength required for large scale applications, with full recentering ability of strains up to 6% [19].

Some researchers implemented SMA wires with carbon fiber laminates in different configurations and ratios, and studied the mechanical behavior of the smart composite [20-21]. Jang et al. [20] discovered that implementing NiTi wires in the CFRP composite reduced the tensile strength from 1300 MPa to 1100 MPa, and as low as 50 MPa, depending on the wires and laminates directions. That was attributed to the fact that material defects were generated in the matrix by embedding the wires, and increasing the volume fraction of the wires may even result in a further decrease in the tensile strength of the composite. The failure strains of the composite ranged from 0.5% to 1.25%. Sharifishourabi et al. [21] fabricated a smart composite consisting of unidirectional carbon fiber epoxy layers laminated with an epoxy layer with SMA wires embedded. The unsymmetrical specimens resulted in very low tensile strengths on the order of 18 MPa. SMA wires were also used in a hybrid (fiberglass/SMA) composite to increase the amount of ductility and elastic energy dissipated of the composite [22]. The cyclic strength of the composite was found to be approximately 360 MPa. The test showed that the SMA–FRP specimen was able to sustain 28% of its strength, even after the rupture of the fiberglass, until 3.8% strain, while the GFRP specimen failed at 1.63% strain.

Furthermore, the concept of using only SMA wires in an epoxy matrix to fabricate the SMA-FRP composite and the effect of the martensitic transformation of the wires on the overall behavior was studied [23]. The composite contained wire volume fractions of 6 and 12% and was tested at different temperatures in monotonic tension test. While the tensile strength of the composite ranged between 58 and 100 MPa, the failure strain ranged between 2% and 6%. Zafar and Andrawes [24] also fabricated and tested pure SMA-FRP composite under cyclic loading. The authors used relatively high volume fraction of SMA wires, of 8.46 and 20.3%. The 20.3% SMA-FRP composite was able to recover strains of 7% with minimal residual

deformation. On the other hand, the 8.46% SMA-FRP composite had 3 % residual strains after load removal.

APPROACH

This study explores the use of superelastic NiTi SMA wires, with a diameter of 0.495 mm, as reinforcing fibers in a thermoset epoxy matrix. The SMA wires are proposed to replace the fibers (glass and carbon) used in manufacturing of conventional FRPs. The new SMA-FRP composite is expected to have recentering ability, good energy dissipation capacity, high ductility, and much higher ultimate strains than conventional FRPs. The composite specimens with different reinforcing ratios were fabricated and tested under cyclic loading to characterize their behavior. Specimens were cycled at various stress levels, and results were assessed in terms of maximum strains and the dissipated energy in each cycle, equivalent viscous damping and secant modulus.

METHODOLOGY

Materials

SMA fiber-reinforced polymer composite specimens were fabricated for the experimental investigation. The composite specimens consisted of two components: epoxy matrix, which forms the body of the specimen and bonds the SMA wires together, and SMA wires, which reinforce the matrix and provide strength for the composite. The epoxy matrix used in this study was EPOTUF®37-127 thin epoxy adhesive system supplied by U.S. Composites, Inc. The epoxy has a 2:1 resin-to-hardener mixing ratio by volume, pot life of 40 minutes, set time of 6 hours, and complete 100% curing after approximately 6 days according to the manufacturer. The used SMAs were straight roughened superelastic NiTi wires with a diameter of 0.495 mm and supplied by Nitinol Devices & Components, Inc. The austenite start temperature (A_s), which is temperature above which the wires exhibit superelastic behavior, of the wires is -5.5°C

Sample Preparation

To fabricate the specimens, aluminum molds were initially made to secure the wires at the specimen's centerline and fabricate the specimens according to ASTM D638-14 [25], as shown in Figure 1(a). The design of the aluminum mold had a main drawback, that in order to demold the specimens, a screwdriver was needed to push the samples out of the mold. This technique applied bending forces on the specimens and resulted in cracking most of the samples, as shown in Figure 1(b).

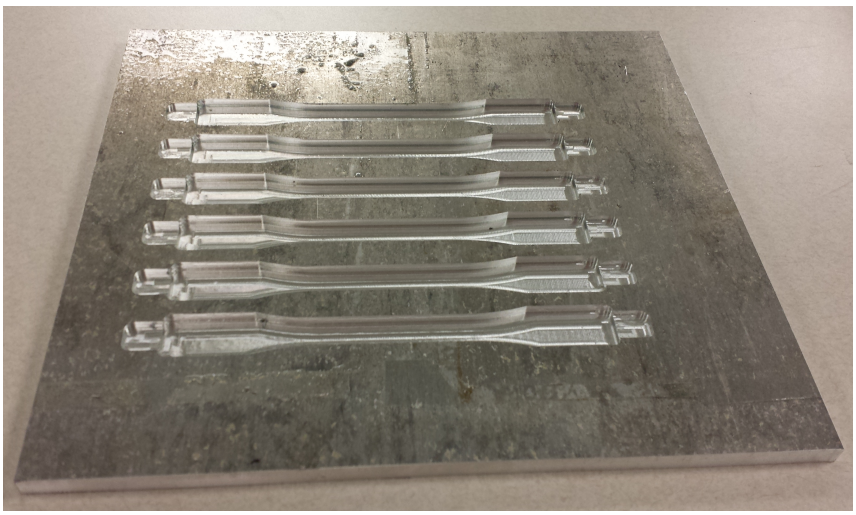

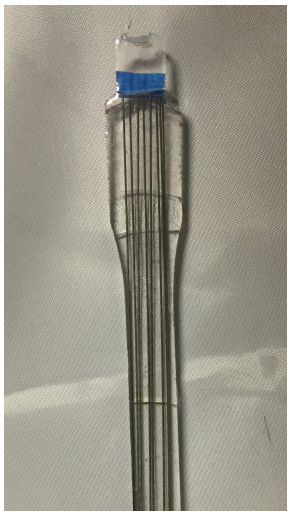

(a) (b)

Figure 1. (a) First design of the aluminum mold; (b) Cracked specimen while being demolded.

As a result, a plastic mold was then designed and fabricated to overcome the main drawback of the aluminum mold. The mold of each specimen consisted of two parts that can be separated during the demolding process without applying any bending forces on the specimens. Figure 2(a) shows the test specimen dimensions with tested cross section area of 13x4 mm^2 and relatively larger area at the gripping zones, while Figure 2(b) shows the redesigned plastic mold.

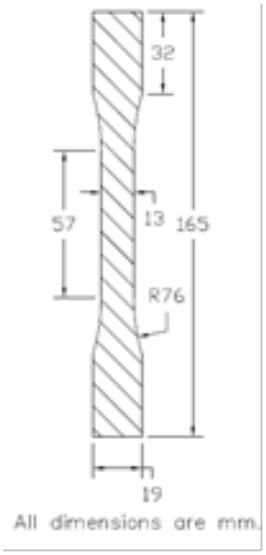

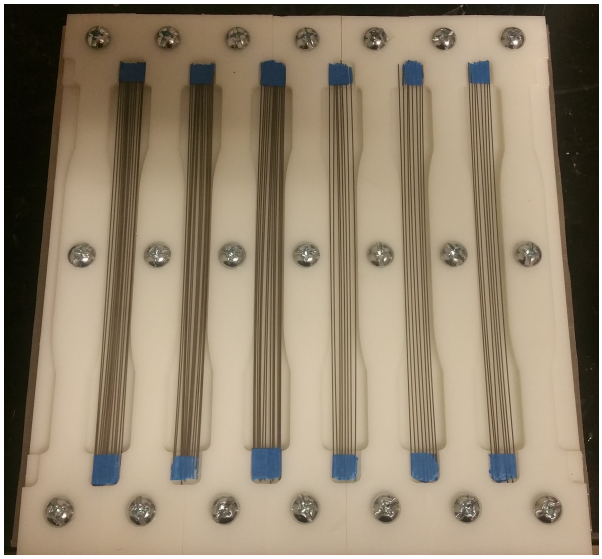

(a) (b)

Figure 2. (a) Dimensions of the test composite specimen; (b) The special plastic mold with aligned SMA wires.

Two sets of SMA-FRP specimens with eight and thirteen SMA wires were prepared. The corresponding fiber volume ratio in those sets were 3.0%, and 4.9%, respectively. The required amount of SMA wires were placed inside the mold and epoxy was poured to fill the specimens. The mold was then covered and sealed using a layer of peel ply for 24 hours. Afterwards, specimens were demolded and left to cure in air and ambient temperature of approximately 25°C and humidity of 50% RH for additional 6 days before it was tested at the age of 7 days

Test Setup

The mechanical behavior of the fabricated composites was investigated under uniaxial cyclic loading. At 7 days, specimens were tested under a cyclic loading protocol in a force controlled mode. At the beginning of the test, the load was ramped to approximately 220 N with loading rate of 10 N/sec. The specimens were then cycled for 3 cycles between this load level and zero force using a loading frequency of 0.01 Hz. By the end of the third cycle, the specimens were again cycled for 3 additional cycles between an increased load level of 440 N and zero force with the same frequency. Following the same procedure, the load was continuously increased by an increment of 220 N, with the specimens cycled 3 times between each load level and zero force with a loading frequency of 0.01 Hz. The load was incrementally increased until the failure of the specimen or reaching 4400 N. The tests were performed in a 98-kN MTS® servo hydraulic machine. Test loads were recorded using the MTS® data acquisition system, and displacements were captured by a laser extensometer, attached to the system over 50 mm gauge length in the middle portion of each specimen. The data sampling rate was 100 Hz. Moreover, CFRP tabs were glued on both sides of the gripping area in each specimen to prevent crushing of this area by the machine grips and enhance gripping during the test. The CFRP tabs consisted of four layers of carbon fibers and were fabricated in the lab using the vacuum assisted hand lay-up technique according to ASTM D5687-07 [26]. Figure 3 shows the test setup with one of the specimens with the CFRP tabs.

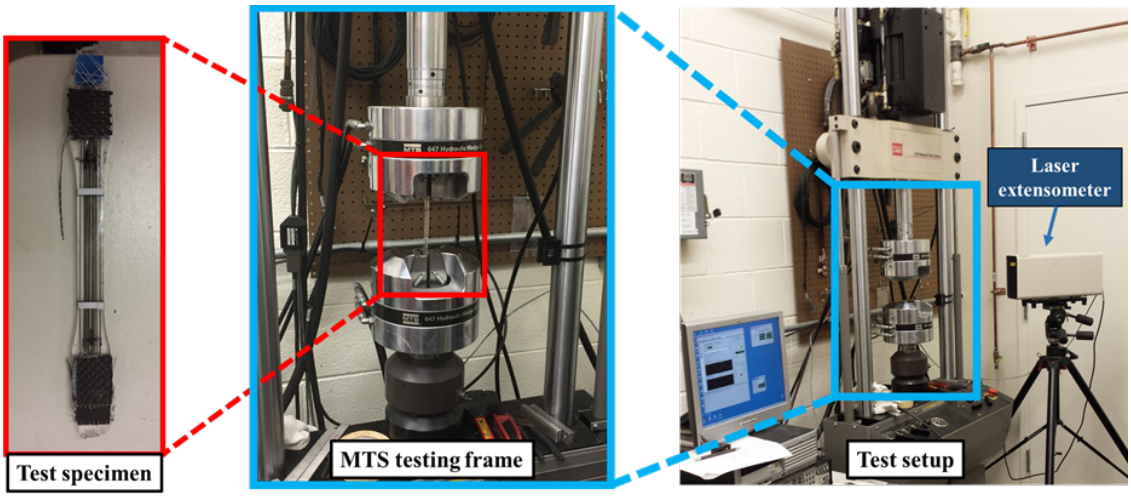

Figure 3. SMA-FRP composite specimen with CFRP tabs, and test setup with the laser extensometer.

Measurements

During the cyclic test, forces and displacements were recorded and uniaxial tensile stresses and strains were calculated. Axial stresses were calculated by dividing the recorded forces by the cross sectional area of the gauge section of each specimen, while strains were evaluated by dividing the displacements, recorded by the laser extensometer, by the gauge length (XX mm) of the specimen.

To compare the results between the two test sets in a quantitative way, the dissipated energy per cycle (ΔW), equivalent viscous damping (ζ_{eq}), and the secant modulus (E_{sec}) were calculated and plotted versus strains. The dissipated energy in any cycle (ΔW) was evaluated by computing the area enclosed between the loading and unloading branches of the stress-strain curve of that cycle. The equivalent viscous damping and secant modulus were defined as ($\Delta W/4\pi W$) and (σ_{max}-σ_{min})/(ε_{max}-ε_{min}), respectively, where W is defined as the energy dissipated in equivalent linear system that has the same maximum and minimum stresses and strains of the load cycle that ΔW was calculated for, σ_{max} and σ_{min} are the maximum and minimum stresses corresponding to the maximum and minimum strains, ε_{max} and ε_{min}.

FINDINGS

Stress-strain Curves

Figure 4 represents the stress-strain curves of the tested specimens under the cyclic loading described. Observing the plots of the two sets, it can be concluded that the loading envelope behavior of the composite followed the well-known plateau of superelastic SMA wires. This indicates that the SMA wires were able to alter the behavior of the pure epoxy (linear elastic to failure) by applying the required reinforcing, and were able to produce the composite action between the wires and epoxy. The response can be divided into three main regions. The first region includes the relatively smaller loading levels with linear elastic behavior of the composite, where strains are fully recovered with approximately zero residual strains. In the last part of the first region, the composite also exhibits the flag-shaped response typical of SMA, characterized with increased strains and full recovery of those strains. The second stage starts then with increasing the load levels, where strains and residual strains are significantly increased under constant load levels. The increase in the residual strains can be attributed to the epoxy matrix. Strains at this stage are believed to be higher than the elastic strains of the pure epoxy. This affects the overall behavior of the composite by imposing plastic deformations in the specimen. With continuous loading and increased strains, the flag-shaped cycles tend to disappear in the third stage. Following the same trend of superelastic SMA wires at this stage, the composite experience minimal increase in the strains with increased loading. The recovered strains at this stage are also very small with relatively high permanent deformations. This stage continues until the failure of the composite specimen.

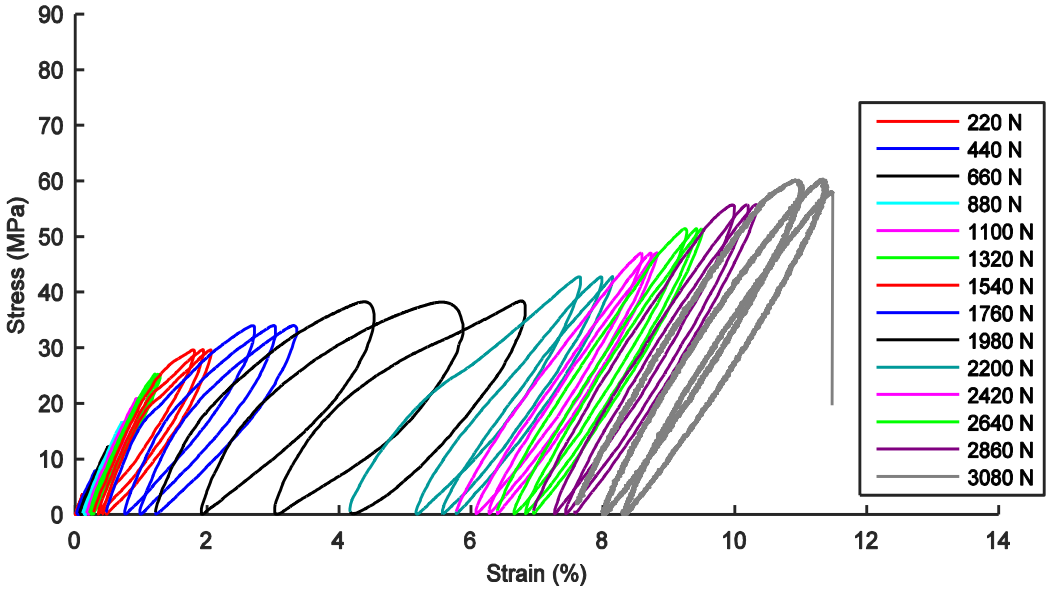

(a)

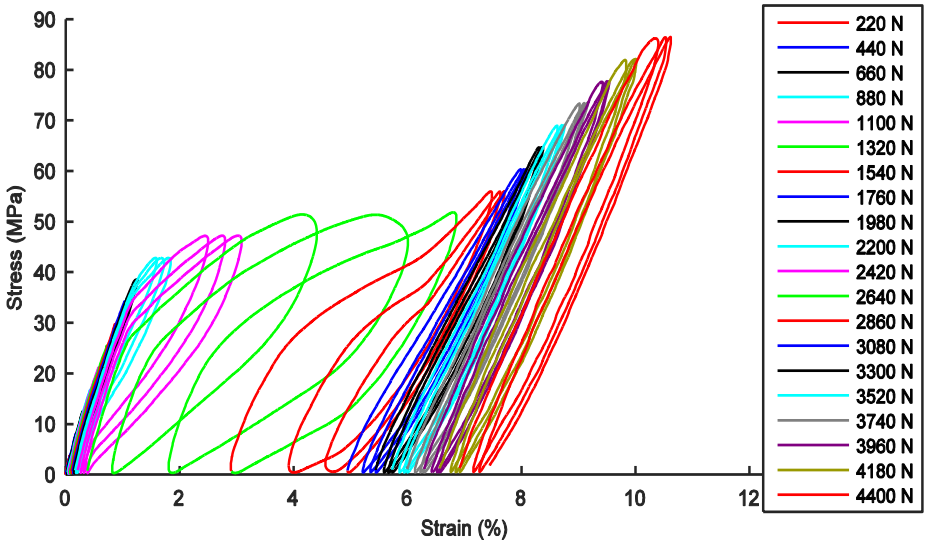

(b)

Figure 4. Stress-strain curves of composite specimens reinforced with: (a) 3.0% SMA, and (b) 4.9% SMA, continuously cycled at various load levels.

To evaluate the effect of changing the SMA reinforcing ratio on the overall behavior of the composite, the start and end stresses and strains of each region for the two sets were calculated and compared, as shown in Figure 5. Starting with the first stage, specimens with 3.0% SMA fiber volume ratio continued to show the linear elastic behavior until 1.29 % strain with associated stress of 25.2 MPa, while the linear elastic part continued to 1.26 % strain under stress of 38.5 MPa in the case of specimens with 4.9% SMA fiber volume ratio.

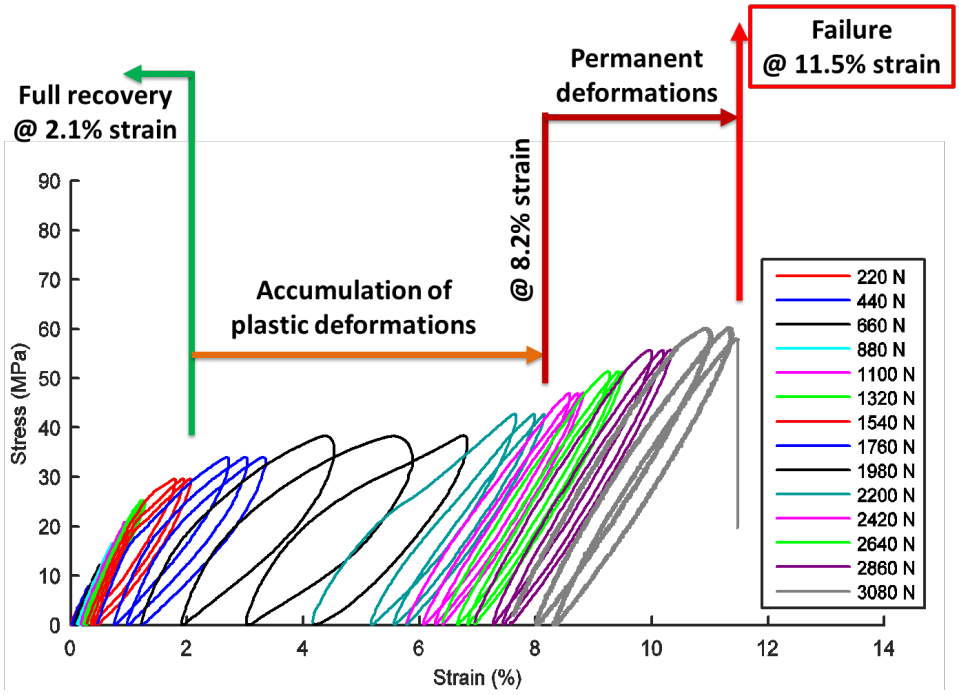

(a)

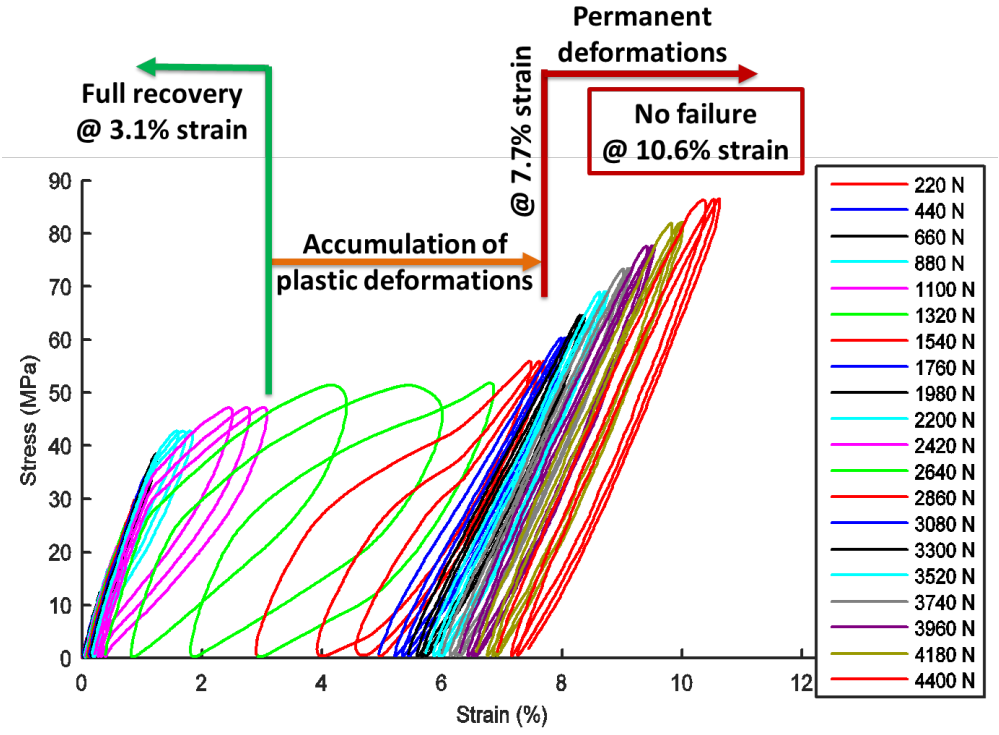

(b)

Figure 5. Comparison between the start and end stresses and strains of each region for specimens with: (a) 3.0% SMA, and (b) 4.9% SMA, continuously cycled at various load levels.

The perfect superelastic behavior of the composite was then exhibited until strains of 2.1 % under stresses of 29.5 MPa for the 3.0 % SMA specimens, and until strains of 3.06 % under stresses of 47.1 MPa for the 4.9 % SMA specimens. The second stage of the 3.0% SMA specimen, with increased residual strains, started from 2.72 % strain with 33.8 MPa axial stresses and continued to 8.16 % strain and 42.7 MPa stress, where the third stage started and continued until failure of the specimen at a strain and stress of 11.49 % and 57.9 MPa, respectively. On the other hand, specimens with 4.9% SMA showed better performance, with the second stage starting from 4.28 % strain with 51.0 MPa axial stresses and continued to 7.71 % strain and 55.9 MPa stress. The third stage for this test set was then started and continued until the end of loading at 86.4 MPa and 10.62 % strain.

Quantitative Properties

Additional specimens from each set were cycled at the load levels that exhibited the superelastic behavior of the composite as shown in Figure 6. Following a similar test procedure, the load was ramped up in a force-control mode to the required load level, with loading rate of 10 N/sec, then the specimen was cycled between that load and zero force for 3 cycles using the same frequency of the first test. The specimen was released from the grips after each test stage and tested again under the next load level. The results of this test stage were consistent with the previous test, where specimens with 3.0 % and 4.9 % SMA fiber volume ratio exhibited perfect superelastic behavior until 2.36% and 3.49 % strains, respectively. Figure 7 represents the variation of the dissipated energy, equivalent viscous damping, and the secant modulus plotted versus strains. For both SMA-FRP sets, the dissipated energy and viscous damping were increased with increasing the strains, and secant modulus was decreased. The increase in the energy and damping with strains can be attributed to the increase in the hysteresis area due to the shift in the composite behavior from linear elastic to superelastic; while the decrease in the secant modulus was expected with the relatively large increase in the strains with each constant increase in the load level. On the other hand, the specimens with higher SMA reinforcement ratios showed better recentering capacity, higher dissipated energy and secant modulus, and higher equivalent viscous damping at larger strains.

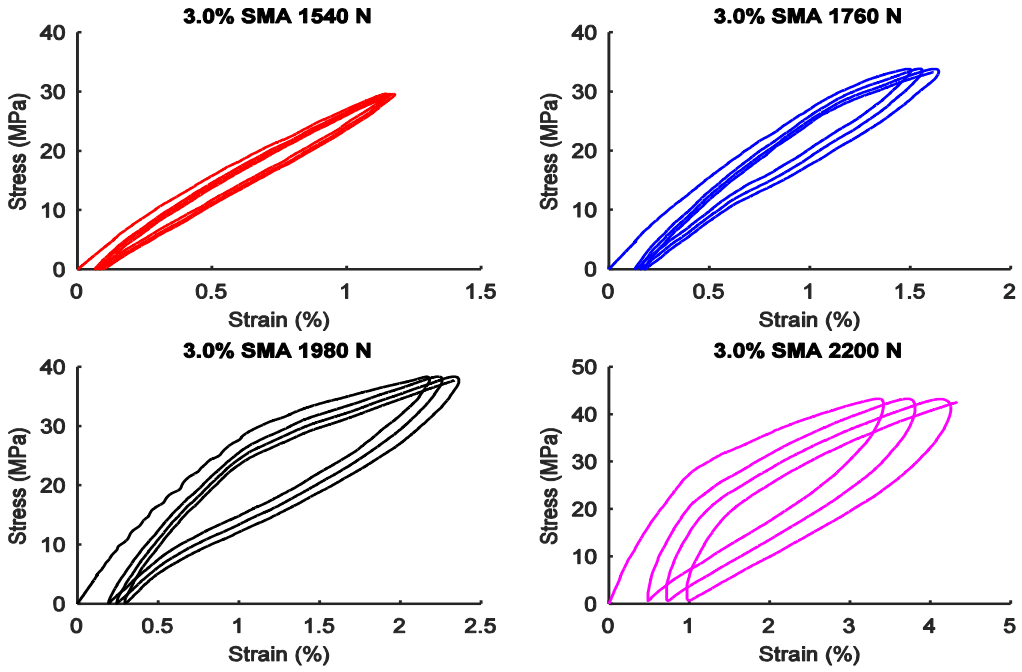

(a)

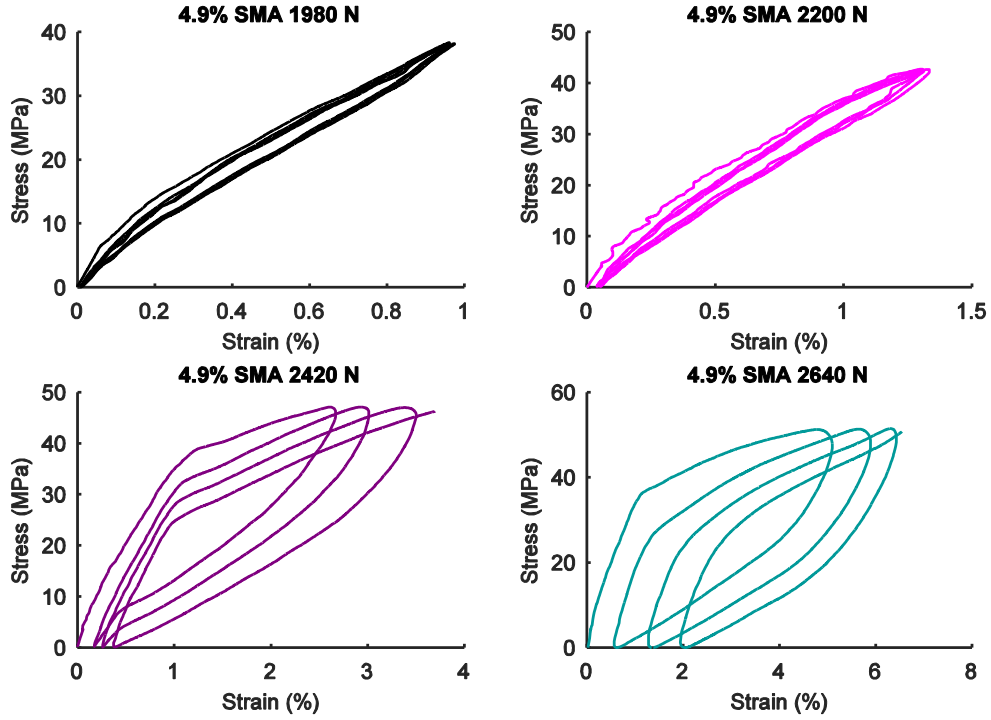

(b)

Figure 6. Stress-strain curves of composite specimens reinforced with: (a) 3.0% SMA, and (b) 4.9% SMA, separately cycled at various load levels.

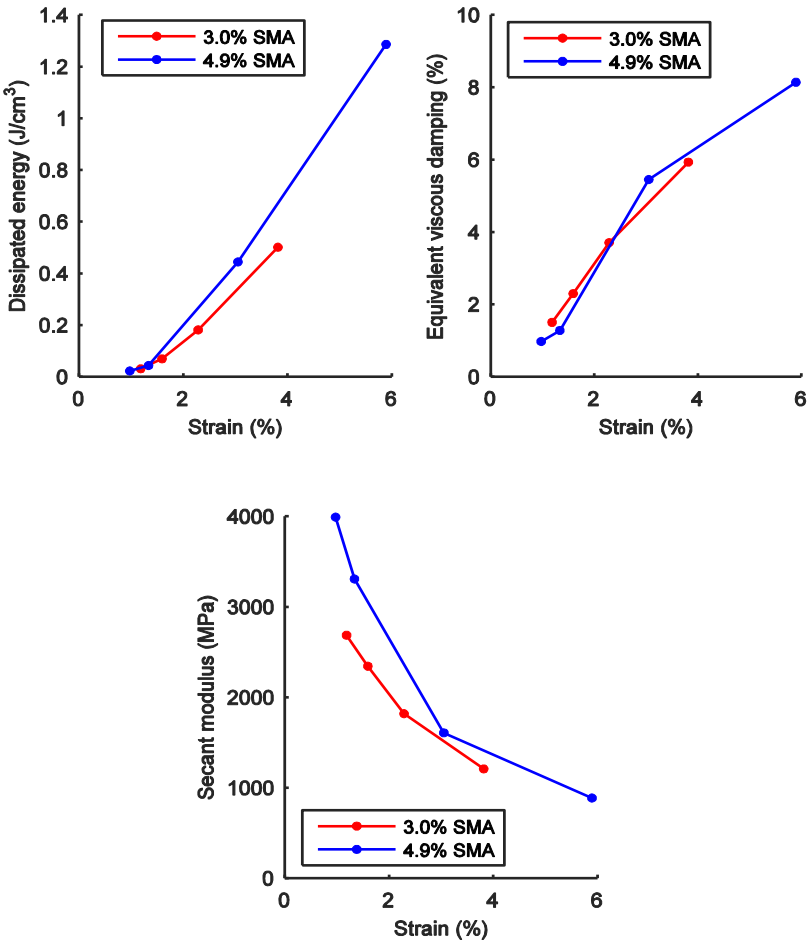

Figure 7. Dissipated energy, equivalent viscous damping, and secant modulus of the tested composite as a function of strain amplitude.

Composite Behavior and Failure Modes

Finally, it is important to understand the behavior of the bond between the SMA wires and the epoxy as it is one of the main factors that defines the interaction between them and hence defines the overall behavior of the composite. Under uniaxial tension loads, both the wires and the epoxy are elongated by the same strain level. But at the same strain level, stresses in the SMA wires are expected to be much higher than the stresses in the matrix, due to the fact that the wires have a larger Young's modulus compared to the matrix. Under increased stresses with continuous loading, the martensitic transformation would be initiated in the wires with continuous elongation, to maintain the global strain level of the specimen, and simultaneous decrease in the wires' diameters. On the other hand, the reinforcing SMA wires are constrained by the matrix. Therefore, the transformation, combined with a decrease in the diameter, will partially take place over several points in each wire, and not completely over the whole embedment length [23]. This phenomenon was observed during the test as debonded areas at the interface between the wires and the matrix. Figure 8(a) shows one of the specimens with gray-colored spots on the wires representing those debonded areas. The bond in the debonded

areas were not recovered during unloading; and with another stage of loading with higher load level, the transformed length continuously increased and debonded areas propagated over the wires. In failed specimens, failure occurred when the debonded areas increased significantly, and the epoxy could not sustain the stresses. The epoxy was fractured at a horizontal section. The epoxy fracture was combined, in most cases, with slippage of the wires from the epoxy, as shown in Figure 8(b). In some cases, the epoxy failure was combined with fracture of some wires and slippage of the unbroken ones.

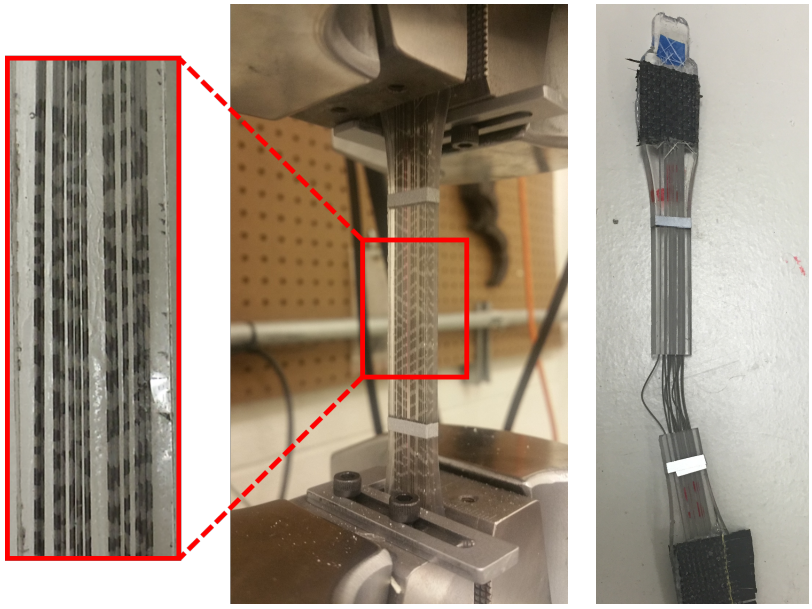

(a) (b)

Figure 8. (a) Gray-colored spots on the wires representing the debonded areas; (b) Failure mode of one of the tested specimens.

In general, test results and failure modes confirmed the composite action between the SMA wires and the epoxy matrix. The ability to fully recover strains until approximately 3.5% and partially recover high strains of approximately 7%, proved the influence of SMA fiber ratio on the composite behavior. The effect of fiber volume ratio can also be seen from the increased dissipated energy, viscous damping and secant modulus with increasing reinforcement ratio.

SHAPE MEMORY ALLOY FIBER REINFORCED MORTARS

PROBLEM

Structural integrity of reinforced concrete bridges highly depends on concrete durability, strength and resistance to cracking. Enhanced ductility and deformation recovery of reinforced concrete allow for less repairs and longer service life. New materials and construction methods are being developed for rehabilitation of existing and design of new bridge structures.

Fiber Reinforced Concrete (FRC) is a fast growing field in the civil engineering industry, and it has been used as a building material in numerous structural applications. Tensile and flexural capacities of FRC are greatly enhanced compared to unreinforced concrete [27]. Moreover, the addition of fibers significantly improves concrete post-cracking behavior [28]. FRC displays increased resistance to cracking, greater control of crack size and its propagation. Consequently, the penetration of harmful solutions into the concrete is greatly inhibited, impeding reinforcement corrosion. One of the most common types of fibers used for concrete reinforcement is steel fibers, which significantly improve mechanical performance of concrete [29]. Frequently, steel fibers are made with hooked ends to provide better anchorage and increase bond strength between fibers and concrete matrix. Steel fibers considerably enhance concrete durability and flexural toughness and strength [30]. After formation of the first concrete crack, steel fibers start absorbing the deformation energy and help reduce the crack propagation, often displaying a deflection hardening behavior. However, beyond yielding, steel fibers deform permanently and do not have a capacity to reduce already formed cracks [31].

The integration of smart materials such as SMAs in concrete structures to enhance post-event functionality has been explored by a number of researchers (9). Abdulridha et al. [33] experimentally studied the behavior of superelastic shape memory alloy reinforced concrete beams. The beams reinforced with SMA bars showed superior response in limiting residual displacements and crack widths as compared to those reinforced with conventional deformed steel bars. Shrestha et al. [34] examined the feasibility of using Cu-based SMAs as longitudinal reinforcement in concrete beams. The cyclic loading test results showed that SMA-reinforced beams have very good recentering capability and provide substantial crack recovery capacity.

Saiidi et al. [35] studied the use of SMA material as reinforcement in the plastic hinge regions of concrete bridge columns. The project investigated the influence of SMA reinforcement and Engineering Cementitious Composite (ECC) concrete on recentering and energy dissipation capacities of bridge structures during a seismic event. Initially, one SMA reinforced concrete column was subjected to an earthquake record on a shake table. Then, the damaged column was repaired with the ECC material and tested again. It was found that both original SMA-reinforced and SMA-reinforced ECC-repaired columns displayed minor residual displacement and post-yield deformation.

A number of studies have been conducted to investigate the effect of SMA fibers in cementitious composites. Choi et al. [36] studied different types of NiTi SMA short fibers, fiber bond strength and crack-closing capacities. Third-point flexural bending tests were conducted

on small beams with five straight or dog-bone shaped SMA fibers with different un-bonded lengths. The fibers were placed over a small notch in the center of the beam about 6 mm from the bottom. Heat was applied to the exposed SMA fibers after deformation to activate their shape memory effect properties. It was concluded that dog-bone shaped fibers had higher bond strength, allowing for better anchorage to concrete; and larger un-bonded lengths showed greater crack-closing capacity. Kim et al. [37] performed pullout tests of single SMA fibers to observe their bond strength and slip properties. It was determined that cold-drawn and heat-treated SMA fibers performed better than the original SMA fibers.

Li et al. [38] studied the ability of NiTi SMA fibers to dissipate energy and self-repair under cyclic third-point flexural loading. The study investigated the performance of SMA fibers with ECC concrete, which exhibits strain-hardening behavior and has a very tight multiple cracking pattern. Six seven-strand SMA cables were placed at the bottom of the specimen across the whole beam length. The SMA cables were pre-strained and anchored before the testing. It was observed that during unloading SMA reinforced specimens significantly recovered the mid-span deflection, and demonstrated crack recovery.

Sun et al. [39] investigated installation methods of SMA wires such as external mounting and embedded SMA wires; and effects of un-bonded wire length on crack recovery. The externally mounted SMA wire application had better crack repair behavior compared to the embedded method, but it was more difficult to implement. In addition, it was concluded that the larger the un-bonded length, the greater crack recovery capacity can be achieved.

The SMA fibers were aligned in the direction of the applied load in most of the previous work. In particular, they are intentionally placed on the tension side of the beam were the flexural cracks form. It is expected that the effectiveness of a group of fibers aligned parallel to the applied stress will be higher than that of the same group of fibers with 2-dimensional random orientations, at least for the straight fibers. It was concluded that further research is needed to study the effectiveness of randomly distributed SMA fibers in cementitious composites.

APPROACH

In this study, the behavior of mortar mixtures with randomly distributed superelastic shape memory alloy (SMA) fibers was investigated. SMA-fiber reinforced mortar beam specimens with 0.25%, 0.5%, and 1% SMA fiber volume ratios were prepared along with a control plain mortar specimen. For the 0.5% fiber volume ratio, two different lengths of SMA fibers were used. Flexural cyclic tests were conducted on both the mortar and concrete beam specimens. The digital image correlation method was used to measure full-field deformations and monitor the damage evolution on the surface of the specimens. Test results were analyzed in terms of flexural strength capacity, mid-span deflection, crack width, fiber distribution and re-centering and crack recovery ratios for each specimen.

METHODOLOGY

Materials and Specimen Preparation

The mortar mixture design and specimen preparation were based on the ASTM C348–02 standard [40]. The ratios of Portland cement to sand and water to cement (w/c) were 1:2.75 and 1:2.10, respectively. The 0.35-mm diameter superelastic strands were used as SMA fibers for mortar mixtures. Each strand consisted of seven NiTi wires with a diameter of 0.117 mm. Three different SMA fiber ratios, namely 0.3%, 0.5% and 1.0% by volume of the mortar, were considered. Each SMA fiber had a length of 30 mm. To assess the effect of SMA fiber length on the performance of the composite, the SMA fibers with a length of 20 mm were also used at 0.3% fiber volume ratio. Therefore, including the control specimen, which consisted of plain mortar, five different mixtures were prepared as shown in Table 1. Three prismatic specimens with dimensions of 40 × 40 × 160 mm were cast from each mixture. The mixing procedure for the SMA fiber reinforced mortar specimens consisted of weighing the required mortar material for each volume fraction and fiber length, and then adding the fibers to the mortar base and mixing once again until the composite material achieved homogeneity. All samples were consolidated using a vibrating table, and covered with plastic and insulated inside styrofoam containers for the first 24 hours. The samples were removed from the molds and cured inside a moisture room (XX °C at 100% RH) for 28 days.

Table 1. Mortar specimens

Specimen	SMA Volume Ratio (%)	SMA Fiber Length (mm)
M-Control	-	-
M-SMA-1	0.3	20
M-SMA-2	0.3	30
M-SMA-3	0.5	30
M-SMA-4	1.0	30

Test Plan and Setup

The SMA fiber-reinforced mortar specimens were loaded under displacement-control in a three-point cyclic flexural testing confirguation. An MTS loading frame with a capacity of 1000 KN was used for the flexural tests. A cyclic loading procedure, which included 13 cycles with a displacement increment of 0.2 mm for each subsequent cycle and a total displacement of 1.4 mm was implemented for all tests. Figure 9 illustrates the cyclic loading pattern. The loading and unloading rate was set to be 1.0 mm/min.

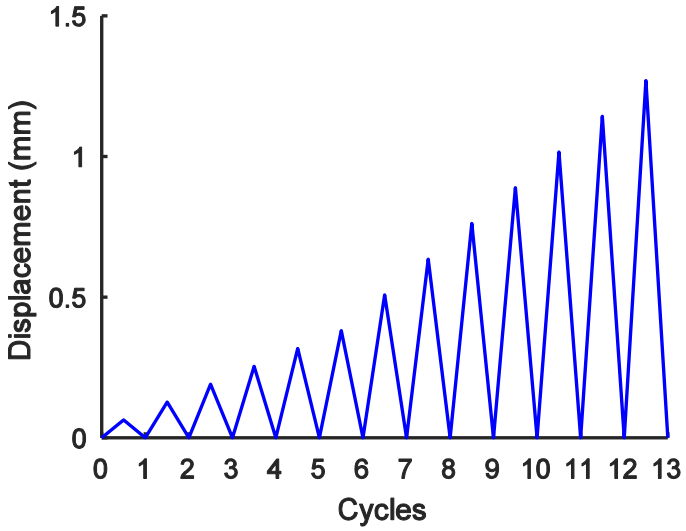

Figure 9. Cyclic loading procedure for fiber reinforced mortar

A two-dimensional digital image correlation (2D-DIC) system was used during the experiments to monitor strain evolution and deformation fields. DIC is a full field and non-contact optical measurement system that can be used to measure strain and deformation from a sequeuce of images during a mechanical testing procedure. The DIC can be used to capture three-dimensional or two-dimensional images based on the number of optical cameras used during the tests and their placement angles. The DIC system can also be used to monitor crack propagation and crack width. To enable the DIC measurements, the surface of specimens needs to be textured with a speckle pattern. DIC tracks the movement of the applied speckle pattern by analyzing the displacement of a speckle, a group of speckles and the pattern within an identified grid. The maximum correlation in each frame corresponds to the displacement vector. Here, a two-dimensional DIC system was used as there was no significant out-of-plane movement. In addition to the DIC measurements, a laser extensometer was used to monitor the specimen deflection on the tension side. Figure 10(a) and (b) shows the test setup for the flexural testing of mortar specimens and the speckle pattern captured by DIC.

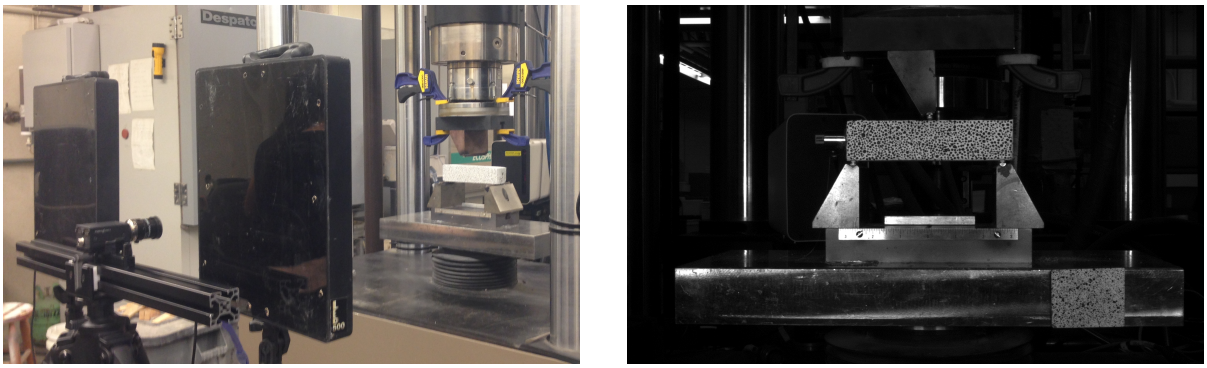
Figure 10. (a) Mortar flexural test setup; (b) Mortar speckle pattern captured by DIC

FINDINGS

Force-displacement curves

Figure 11 displays the cyclic force-displacement curves of the five different types of mortar mixtures. For each mixture type, the result from one specimen was illustrated. The plain mortar specimen (M-Control) and the specimen with 0.3% of 20mm-long SMA fibers (M-SMA-1) failed during the 7th loading cycle. The ultimate strength for the specimens with 0.3% and 0.5% of 30-mm long SMA fibers (M-SMA-2 and M-SMA-3) occurred during the 8th loading cycle. The specimen with 1.0% of 30-mm SMA fibers (M-SMA-3) failed at the 9th cycle and had an ultimate strength at the 5th loading cycle. All specimens developed one main crack at the center of the tension side. The specimens M-SMA-2 and M-SMA-3 had higher flexural strength than the other specimens after the initiation of the first crack. After the first crack, the specimens M-SMA-2 and M-SMA-3 had an increase in flexural strength, indicating a ductile failure pattern. The M-SMA-1 and M-SMA-2 specimens lost 70% and 85% of their ultimate strength in the cycles following post cracking, while the M-SMA-3 specimen had only 12% decrease in its peak force.

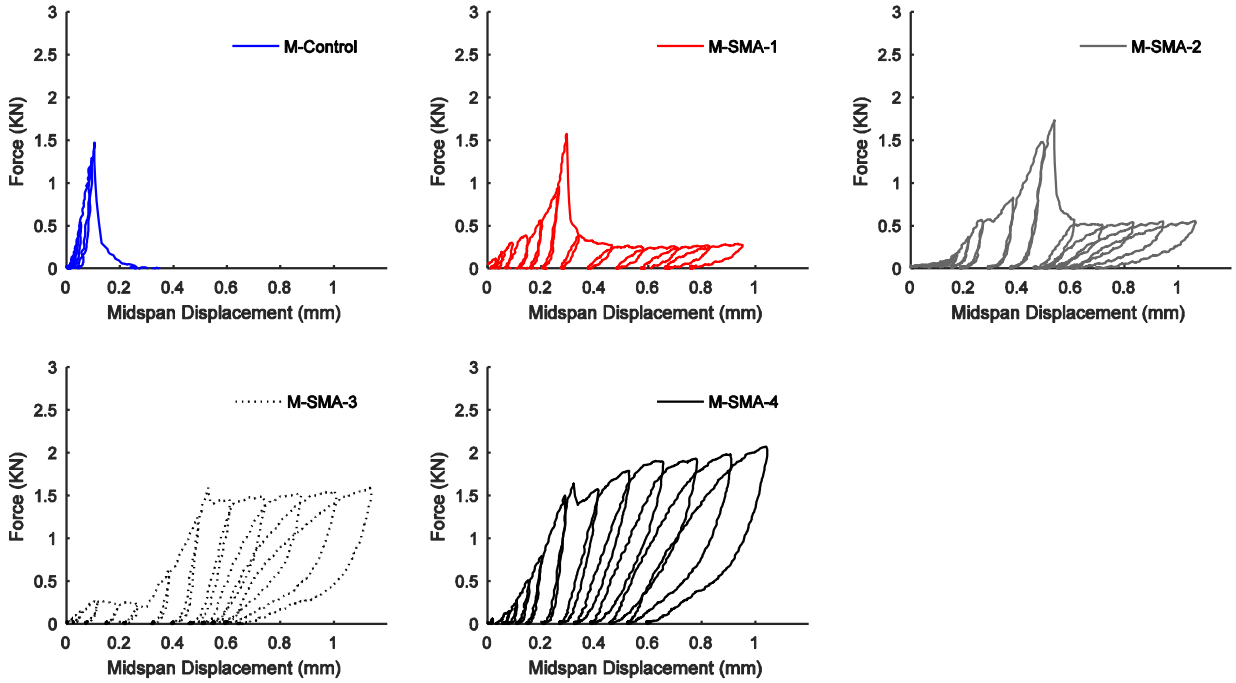

Figure 11. Mortar force-displacement cyclic curves

Envelope curves

Figure 12 illustrates the bending test envelopes of the mortar specimens discussed in Figure 11. The addition of fibers to the mortar mixture increased the overall ductility of the composites, but decreased the flexural stiffness up to a certain fiber content (0.5% SMA in this case). All the

SMA fiber reinforced specimens exhibited a post-cracking residual strength with a minimum of 17% of its peak strength for the M-SMA-1 specimens and a maximum of 126% of its peak strength for the M-SMA-4 specimens as shown in Figure 13.

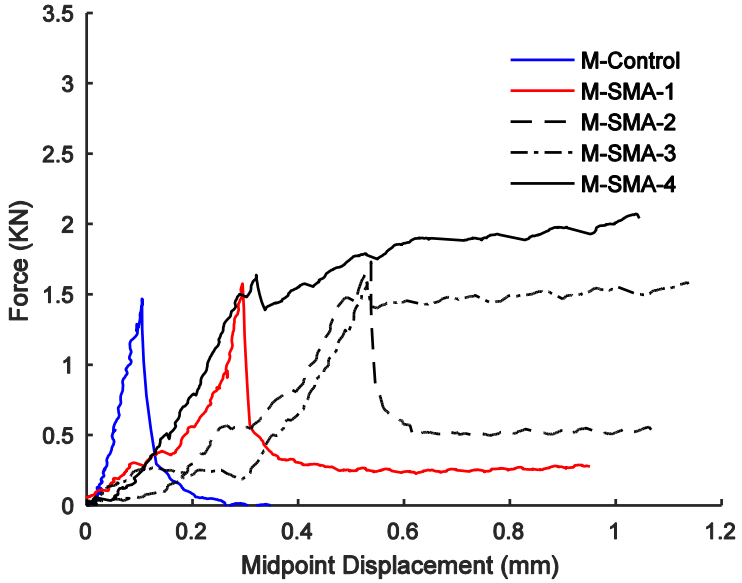

Figure 12. Fiber reinforced mortar force-displacement envelope curves

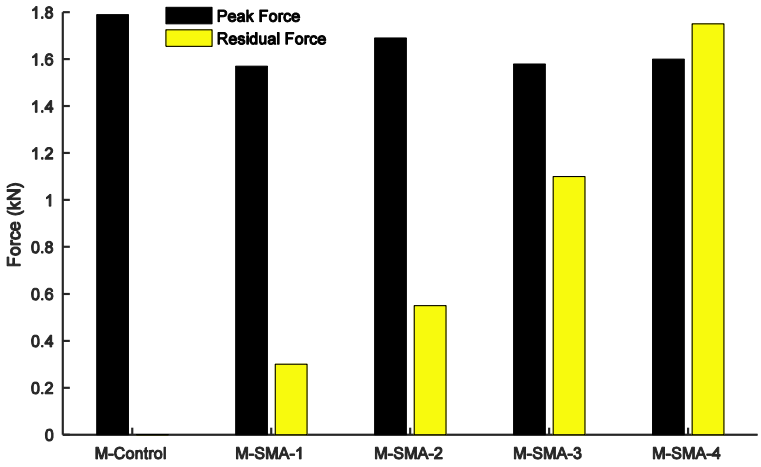

Figure 13. Fiber reinforced mortar peak and residual force

Re-centering capability

The mid-span displacement of the specimens during the cyclic tests was monitored and recorded by the DIC. The average deflections at the end of loading and unloading cycles for

each mixture type were computed and plotted in Figure 14. Figure 14 also illustrates the re-centering ratio (i.e. the ratio of displacement recovered upon unloading to the maximum displacement encountered) for each cycle, which is defined as

$$R = \frac{D_{\max} - D_{residual}}{D_{\max}} \quad (1)$$

where D_{max} is the maximum displacement for each loading cycle and $D_{residual}$ is the residual displacement at the end of each loading cycle. It is observed that the SMA-fiber reinforced specimens had a minimum of 26% recovery at the end of each cycle. After several initial elastic cycles, residual deflections start to occur in the specimens. However, the SMA-fiber reinforced specimens recover most of their deformations that occurred at a given loading cycle at large displacement amplitudes. This can be attributed to the superelastic strains developed in the SMA fibers. The M-SMA-2, M-SMA-3 and M-SMA-4 displayed approximately stable re-centering capabilities after cycle 4 reaching a stable recovery ratio of approximately 35%; while for the M-SMA-1 specimens, the re-centering ratio was gradually decreasing with the increasing number of cycles. That might be due to the shorter SMA fiber lengths in M-SMA-1 specimens, which might induce large unrecoverable strains in the SMA fibers at larger deformation levels.

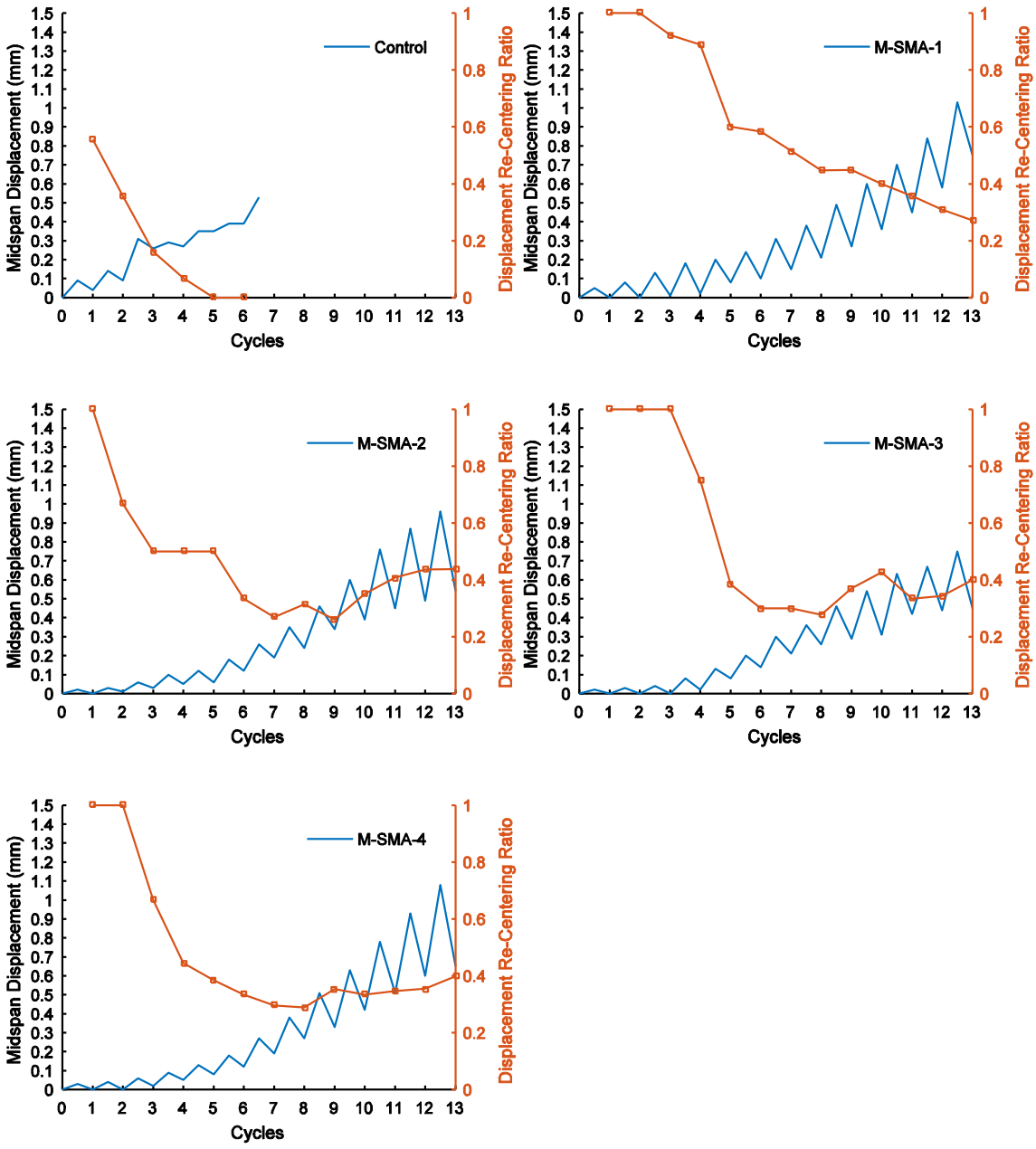

Figure 14. Midspan displacement history and recovery ratio for mortar specimens

Strain Evolution

DIC was used to compute the strain evolution and crack width propagation in the mortar specimens. The evolution of the longitudinal strain contours for the SMA fiber reinforced mortar specimens are illustrated at four stages of the test. Figure 15(a) shows full-field strain measurements at the first crack. Figure 15(b) demonstrates full-field strain measurements at the peak load. The strain evolutions at the peak load of the last loading cycle and at the end of the testing procedure (i.e. after the unloading of the last cycle) are given in Figure 15(c) and Figure 15(d), respectively. It can be seen that the M-SMA-1 specimen experienced larger and

more widely distributed strains at each phase of the loading compared to other SMA fiber reinforced specimens. At the peak load of the last (13th) cycle (Fig. 6c), the strain distributions across the M-SMA-1 specimen was the highest, followed by the M-SMA-3, M-SMA-2, and M-SMA-4, respectively.

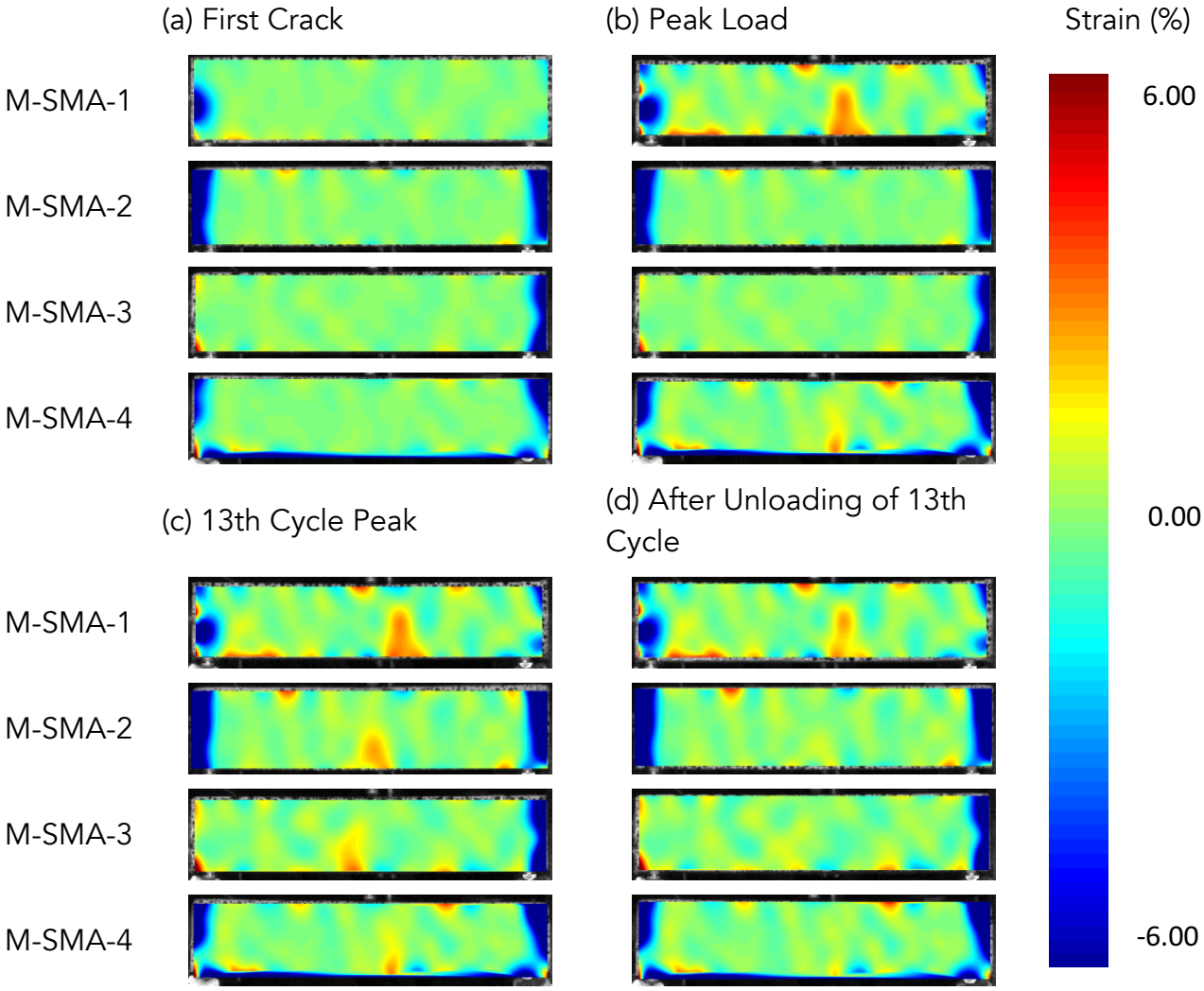

Figure 15. Full-field strain measurement of SMA fiber reinforced mortar using 2D DIC (a) at the first crack; (b) at the peak load; (c) at the 13th cycle peak and (d) after unloading of 13th cycle.

Crack-Width Propagation

The DIC was also used to monitor the crack width propagation in the mortar specimens. Figure 16 shows the average crack propagation history for various mortar mixture types. It can be seen that the crack recovery occurred after the 7th cycle for all SMA mortar specimens. The control specimen failed at the 9th cycle with a crack width of 5.5 mm. Although the specimens with 0.5% of 30-mm SMA fibers had the least residual displacement at midpoint, the specimens with 1.0% of 30-mm SMA fibers had the least crack propagation and the highest crack recovery ratio

(i.e. the ratio of the crack width at the peak load to that at unloading for each cycle). The specimens with 0.3% of 20-mm SMA fibers had a similar crack propagation profile to the specimens with 1.0% of 30-mm SMA fibers, but they failed during the loading phase of the 13th cycle. The analysis of the experimental results for the mortar fiber reinforced specimens suggests that the 1.0% SMA 30 mm, 0.3% SMA 20 mm and 30 mm can be used for controlling crack propagation.

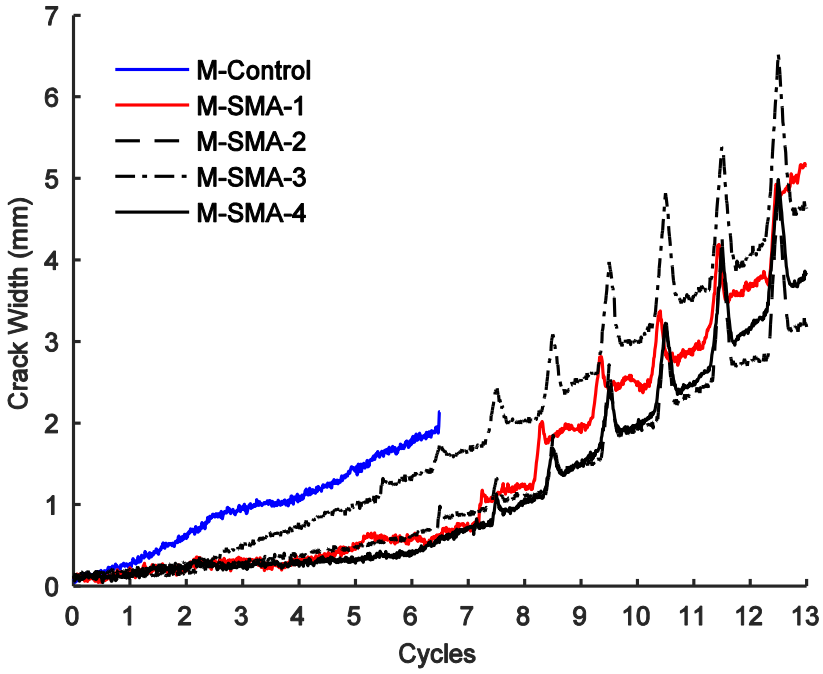

Figure 16. Mortar crack width history

CONCLUSIONS

This project investigated the development of advanced composite materials that can be incorporated into transportation infrastructure for more adaptive and resilient response under extreme weather events. In particular, shape memory alloys, which are a metallic alloy with various advantageous mechanical characteristics, are used as fiber to develop two types of composite materials: (i) shape memory alloy fiber reinforced polymers and (ii) shape memory alloy fiber reinforced mortars.

To develop a SMA-fiber reinforced polymer, superelastic SMA wires used as reinforcing fibers in a thermoset epoxy matrix. The SMA-FRP samples was fabricated and tested. Test sets included composite specimens reinforced with 3.0% and 4.9% SMA fiber volume ratios. The specimens were tested under incrementally increased uniaxial tensile cyclic loads in a force-controlled mode test. Test stresses and strains were calculated for evaluation. The findings of the experimental tests can be summarized as follows:

- Specimens with higher reinforcement ratios showed better behavior in recovering large strains, dissipating energy, and having higher equivalent viscous damping and secant modulus.
- Specimens with 4.9% SMAs were able to fully recover strains up to 3.5% and partially recover 6% strains with 2% residual deformations.
- Compared to the other SMA/CFRP, SMA/GFRP, or SMA/epoxy composites, the fabricated SMA-FRP composite showed a comparable tensile strength and ability to recover strains, with the use of only 4.9% SMAs.
- The overall behavior of the composite can be further enhanced by using higher volume fraction of SMA wires with larger wires' diameter to eliminate the possibility of having a condensed coupon.

To develop a SMA-fiber reinforced mortar, the SMA fibers were added at 0.3%, 0.5% and 1.0% volume ratios. Flexural cyclic loading tests were conducted on mortar beam specimens. During testing, a digital image correlation system was used to monitor the full strain and displacement fields as well as crack propagation. The findings of the experimental tests can be summarized as follows:

- The addition of the SMA fibers increased the overall ductility of the mortar composites. The specimens with 1.0% SMA fibers exhibited deflection hardening behavior, with residual strength up to 26% of their peak strength. All other types of the SMA-fiber reinforced mortars exhibited deflection softening behavior.
- The specimens with 30-mm long SMA fibers showed good re-centering capability at high deformation levels. Increasing the SMA fiber volume ratio from 0.3% to 0.5% considerably improved the flexural performance and re-centering ability of the samples. However, a further increase of the SMA fiber volume ratio to 1.0% did not significantly affect the re-centering behavior. Nevertheless, the specimens with 1.0% of SMA fibers by volume exhibited the highest re-centering ratio, with a minimum of 29% for each loading cycle.
- The specimens with 1.0% of SMA fibers by volume displayed the smallest crack propagation and the highest crack recovery ratio.

RECOMMENDATIONS

Based on the findings of the current study, following recommendations can be made for future research on SMA-FRP composite materials:

- The overall behavior of the composite was affected by the properties of the SMA wires and epoxy matrix. Therefore, the use of different epoxy matrix with a higher elastic strain might be investigated to increase the elastic strain and hence the recentering capacity of the composite.

- In the proposed composite, SMA wires were used as the reinforcing fibers, providing the strength of the composite. Using higher volume fraction of SMA wires are expected to increase the tensile capacity of the smart composite.

Based on the findings of the current study, following recommendations can be made for future research on SMA-fiber reinforced mortar materials:

- Additional work is needed to study the performance of SMA fibers in mortar materials and determine optimum fiber geometry and fiber volume ratio.
- The use of SMA fibers with hooked ends or irregular or crimped surface may provide better mechanical interlock and bond to the concrete and mortar materials as compared to straight fibers.
- The enhanced bond between the SMA fibers and matrix is expected to improve the overall performance of SMA-based cementitious composite systems and will be the focus of future investigations.

REFERENCES

[1] Leonard, K., Hyman, R., and Smith, J. (2014) "Climate Change, Extreme Weather Events and the Highway System: A Practitioner's Guide.", National Cooperative Highway Research Program, Report Number 20-83(5).

[2] Einde, L. V. D., Zhao, L., Seible, F., (2013). "Use of FRP composites in civil structural applications", *Construction and Building Materials*, 17, 389–403.

[3] ACI COMMITTEE 440.2R-08. (2008). "Guide for the design and construction of externally bonded FRP systems for strengthening concrete structures", Farmington Hills: MI, USA.

[4] Morioka, K.; Tomita, Y., (2000). "Effect of lay-up sequences on mechanical properties and fracture behavior of CFRP laminate composites", *Materials Characterization*, v 45, n 2, p 125-36.

[5] Kumagai, S.; Shindo, Y.; Horiguchi, K.; Takeda, T., (2003). "Mechanical characterization of CFRP woven laminates between room temperature and 4 K", *JSME International Journal, Series A (Solid Mechanics and Material Engineering)*, v 46, n 3, p 359-64.

[6] Di Ludovico, Marco; Piscitelli, Filomena; Prota, Andrea; Lavorgna, Marino; Mensitieri, Giuseppe; Manfredi, Gaetano, (2012). "Improved mechanical properties of CFRP laminates at elevated temperatures and freeze-thaw cycling", *Construction and Building Materials*, v 31, p 273-283.

[7] Cree, D.; Gamaniouk, T.; Loong, M.L.; Green, M.F., (2015). "Tensile and Lap-Splice Shear Strength Properties of CFRP Composites at High Temperatures", *Journal of Composites for Construction*, v 19, n 2, p 04014043 (12 pp.)

[8] Kotani, M.; Yasufuku, Y.; Inoue, N.; Kurihara, K.; Kawada, H., (2013). "Lifetime prediction of woven GFRP laminates under constant tensile loading in hydrothermal environment", *Mechanics of Time-Dependent Materials*, v 17, n 2, p 261-74.

[9] Ozbulut, OE, Hurlebaus, S, DesRoches, R., (2011). "Seismic response control using shape memory alloys: A Review", *Journal of Intelligent Material Systems and Structures*, 22:1531-1549.

[10] Morgan, N. B., (2004). “Medical shape memory alloy applications—The market and its products”, *Materials Science & Engineering A*, 378(1–2), 16–23.
[11] Gil, F. J., and Planell, J. A., (1998). “Shape memory alloys for medical applications”, *Proceedings of the Institution of Mechanical Engineers, Part H: Journal of Engineering in Medicine*, 212(6), 473–488.
[12] Mertmann, M., (2004). “Non-medical applications of NITI-NOL.”, *Minimally Invasive Ther. Allied Technol.*, 13(4), 254–260.
[13] Ozbulut, O. E., and Roschke, P. N., (2010). “GA-based optimum design of a shape memory alloy device for seismic response mitigation”, *Smart Materials and Structures*, 19(6), 065004.
[14] Ozbulut, O. E., and Hurlebaus, S., (2012). “A comparative study on seismic performance of superelastic-friction base isolators against near-field earthquakes”, *Earthquake Spectra*, 28(3), 1147–1163.
[15] Dezfuli, F. H., and Alam, M. S., (2013). “Shape memory alloy wire-based smart natural rubber bearing”, *Smart Materials and Structures*, 22(4), 045013.
[16] AlSaleh, R., Casciati, F., El-Attar, A., and El-Habbal, I., (2012). “Experimental validation of a shape memory alloy retrofitting application”, *Journal of Vibration and Control*, 18(1), 28–41.
[17] Miller, D. J., Fahnestock, L. A., and Eatherton, M. R., (2012). “Development and experimental validation of a nickel–titanium shape memory alloy self-centering buckling-restrained brace”, *Engineering Structures*, 40, 288–298.
[18] Daghash, S.M.; Ozbulut, O.E., (2016). “Rehabilitation of Reinforced Concrete Structures Using Shape Memory Alloys*”; Geotechnical and Structural Engineering Congress 2016*, p 685-98.
[19] Ozbulut, O.E.; Daghash, S.; Sherif, M.M.; (2016). “Shape memory alloy cables for structural applications”, *Journal of Materials in Civil Engineering*, v 28, n 4, p 04015176 (10 pp.)
[20] Byung-Koog Jang; Ja-Ho Koo; Toyama, N.; Akimune, Y.; Kishi, T., (2001). “Influence of lamination direction on fracture behavior and mechanical properties of TiNi SMA wire-embedded CFRP smart composites”, *Proceedings of the SPIE - The International Society for Optical Engineering*, v 4326, p 188-97, 2001.
[21] Sharifishourabi, G.; Alebrahim, R.; Sharifi, S.; Ayob, A.; Vrcelj, Z.; Yahya, M.Y., (2014). “Mechanical properties of potentially-smart carbon/epoxy composites with asymmetrically embedded shape memory wires”, *Materials & Design*, v 59, p 486-93.
[22] Wierschem, N.; Andrawes, B., (2010). “Superelastic SMA-FRP composite reinforcement for concrete structures”, *Smart Materials and Structures*, v 19, n 2, p 025011 (13 pp.)
[23] Payandeh, Y.; Meraghni, F.; Patoor, E.; Eberhardt, A., (2012). “Study of the martensitic transformation in NiTi-epoxy smart composite and its effect on the overall behavior”, *Materials & Design*, v 39, p 104-10.
[24] Zafar, A.; Andrawes, B., (2014). “Fabrication and Cyclic Behavior of Highly Ductile Superelastic Shape Memory Composites”, *Journal of Materials in Civil Engineering*, v 26, n 4, p 622-32.
[25] ASTM D638-14, (2014). “Standard Test Method for Tensile Properties of Plastics”, *ASTM International*, West Conshohocken, PA.

[26] ASTM D5687 / D5687M-95, (2007). “Standard Guide for Preparation of Flat Composite Panels with Processing Guidelines for Specimen Preparation”, ASTM International, West Conshohocken, PA.

[27] Kosmatka, SH, and Wilson, ML, (2011). Design and Control of Concrete Mixtures, 15th Edition. Portland Cement Association, Skokie, Ill.

[28] Abrishambaf, A., Cunha, V. M. C. F., and Barros J. A. O., (2015). “The influence of fibre orientation on the post-cracking tensile behaviour of steel fibre reinforced self-compacting concrete”, *Frattura Ed Integrità Strutturale (Fracture and Structural Integrity)*, Vol. 31, pp. 38–53.

[29] Holschemacher, K., Mueller, T., and Ribakov Y., (2010). “Effect of steel fibres on mechanical properties of high-strength concrete”, *Materials and Design*, Vol. 31, No. 5, pp. 2604–2615.

[30] American Concrete Institute, Committee 544. State-of-the-Art Report on Fiber Reinforced Concrete Reported. ACI Committee 544.1R-96. Farmington Hills, Mich., 2002.

[31] Shajil, N., Srinivasan, S. M., and Santhanam M., (2012). “Self-centering of shape memory alloy fiber reinforced cement mortar members subjected to strong cyclic loading”, *Materials and Structures*, pp. 651–661.

[32] Ozbulut, O. E., and Hurlebaus S., (2010). “Neuro-fuzzy modeling of temperature- and strain-rate-dependent behavior of NiTi shape memory alloys for seismic applications”, *Journal of Intelligent Material Systems and Structures*, Vol. 21, pp. 837-849.

[33] Abdulridha, A., Palermo, D., Foo, S., and Vecchio F. J., (2013). “Behavior and modeling of superelastic shape memory alloy reinforced concrete beams”, *Engineering Structures*, Vol. 49, pp. 893-904.

[34] Shrestha, K. C., Araki, Y., Nagae, T., Koetaka, Y., Suzuki, Y., Omori, T., and Ishida K., (2013). “Feasibility of Cu–Al–Mn superelastic alloy bars as reinforcement elements in concrete beams”, *Smart Materials and Structures*, Vol. 22(2), 025025.

[35] Saiidi, M. S., and Wang H., (2006). “Exploratory Study of Seismic Response of Concrete Columns with Shape Memory Alloys Reinforcement”, *ACI Structural Journal*, pp. 436-443.

[36] Choi, E., Kim, D. J., Chung, Y., Kim, H. S., and Jung C., (2015). “Crack-closing of cement mortar beams using NiTi cold-drawn SMA short fibers. Smart Materials and Structures”, Vol. 24, No. 1, pp. 1-11.

[37] Kim, D. J., Kim, H. A., Chung, Y.-S., and Choi E., (2014). “Pullout resistance of straight NiTi shape memory alloy fibers in cement mortar after cold drawing and heat treatment”, *Composites Part B*, Vol. 67, pp. 588–594.

[38] Li, X., Li, M., and Song G., (2015) “Energy-dissipating and self-repairing SMA-ECC composite material system”, *Smart Materials and Structures*, Vol. 24, No. 2, pp. 1–15.

[39] Sun, L., Liang, D., Gao, Q., and Zhou J., (2013). “Analysis on factors affecting the self-repair capability of SMA wire concrete beam”, *Mathematical Problems in Engineering*, pp. 1-6.

[40] ASTM Standard C348, 2002, “Standard Test Method for Flexural Strength of Hydraulic Cement Mortar,” ASTM International, West Conshohocken, PA, 2002, DOI: 10.1520/C0348-02, www.astm.org.